



Power Quality Enhancement Using Evolutionary Algorithms in Grid-Integrated PV Inverter

N. Vanaja¹ · N. Senthil Kumar¹

Received: 7 August 2022 / Revised: 11 February 2023 / Accepted: 16 February 2023 / Published online: 11 March 2023
© The Author(s) under exclusive licence to The Korean Institute of Electrical Engineers 2023

Abstract

Researchers are now concentrating on the problem of finding the optimal P–Q control of real and reactive power in grid-connected inverters with the emergence of Solar PV systems. The provision of both real and reactive power is essential for the improvement of overall power quality; in addition to maintaining grid voltage and power factor, grid-interlinked inverters are seen as the most cost-effective means of compensating for real and reactive power. In various ecological settings, photovoltaic systems are linked to the power grid to deliver reactive power. This paper proposes the decoupled P–Q model with the Salp swarm optimization technique to manage the Grid-tied inverters. Moreover, the proposed controlling techniques reduce Total Harmonic Distortion (THD) and output controlled power more efficiently than existing controllers. Moreover, THD is calculated and exhibited. Numerical simulations demonstrate that SSO and PSO algorithms can resolve a harmonic elimination problem just as effectively as GA. When compared to SSO, PSO yields numerical simulation outcomes that are steadier and feature a smaller standard deviation. A 75 kW grid-linked converter is modelled and tested in a simulation study with MATLAB Simulink to prove the efficiency of the system. Utilizing the MATLAB Software, the proposed Salp swarm optimization approach is compared to conventional optimization approaches such as PI controller, GA, and PSO. The results of the traditional feedforward controller are compared with the suggested SSO technique in a variety of cases. A low-scale prototype model is also created for real-time implementation to authenticate the outcomes of the simulations.

Keywords Solar PV · Grid-integrated inverter · Real and reactive power · Salp Swarm Optimization (SSO) · Genetic Algorithm (GA) · Particle Swarm Optimization (PSO) · Proportional Integral controller (PI)

1 Introduction

Power electronics is being used to connect integrated renewable energy sources such as solar panels and wind generators into power systems. When unexpected power unbalances occur, huge magnitude frequency fluctuations in power distribution systems have a significant impact on sustainable power. The principal causes of all these frequency variations are a shortage of angular momentum in power converters and the intermittent nature of sustainable power. The angular momentum of massive synchronous machines stabilizes the frequency deviation in traditional power distribution systems.

The fuzzy inference system model is built and utilises an evolutionary algorithm-based metric. The controller works by raising the VSM velocity to enhance non-synchronous supply saturation. When frequency range and ROCOF are high, this novel VSM method improves the microgrids' dynamic resonance frequency, resulting in lower overall microgrids. The Logistic regression approach is employed in a profitability evaluation model to reconcile operator income optimization with voltage fluctuation constriction while employing the power compensating control system. This technique's effectiveness is checked using a single-stage three-phase grid-interlinked PV system with various testing scenarios.

Multi-level converters can be employed to attach wind turbines to grids; the controller must be able to transmit an unequal amount of power to the networks, preventing the DC link [5, 6] of the converter from worsening. A minimal power method that tackles the resource management issue by employing a chart methodology gives a new method for

✉ N. Vanaja
vanajamsec@gmail.com

¹ Department of Electrical and Electronics Engineering,
Mepco Schlenk Engineering College, Sivakasi, Tamilnadu,
India

finding the best control system operations. Reformed Electric System Cascade Analysis enhances the faults mentioned earlier. The real-world example displayed upon the implementation of Reformed Electric System Cascade Analysis demonstrates the optimal solution technology's convenience and reliability in overcoming significant problems of the traditional linear programming being used [1]. In a book exploring human behavior in various scenarios, a Human Psychology Optimal (HPO) approach is proposed for the comprehensive monitoring of a partially shaded Photovoltaic system. The HPO approach is driven by the main purpose of examining users' psychological and emotional processes. Some essential elements of Human Psychology Optimization are emotion-related processes such as exhilaration, eagerness, learning, identity, nervousness, and over-excitement [4].

A Cascaded Multilevel Inverter's primary function is to synthesise the desired voltage using different DC sources such as battery packs or photovoltaic panels. The Cascaded Multilevel Inverter is said to be symmetric, whereas DC bus voltages of the HBs are identical. Because Photovoltaic solar outputs vary according to ecological conditions, unbalanced inverters were recommended. Therefore, the asymmetric inverter's DC/DC converter voltages differed [2, 3].

Comprehensive research was conducted to bolster the reliability of a grid-connected PV system, with consideration of various parameters such as the number of failure and recovery levels of every electric system element, the amount of Photovoltaic system, the rated capacity produced on each Solar panel, and the PV system's installation position in the power grid. However, incorporating these parameters into the target parameters made the systems excessively complex and difficult to manage for any optimization technique. Thus, the schematic approach and MCT were utilized to ease the integration of these components in the optimum solution [10]. To reduce the amount of darkened cells and, as a result, increase the overall device electrical output. A maximum power point tracking approach has been used to get the highest potential electrical output, which is only a Perturb augmented and Observe Algorithm. The suggested method employs Pareto evaluation dependent on incoming meteorological data [4]. The proposed approach utilizes a continuous backtracking technique suitable for forecasting errors by changing real control activity in light of a new pursuit done at each time [11]. The proposed multi-objective model's different methodology is characterized. The multi-situation ideal arrangement with a separated wellness work is reworked through a simple to-fathom uncertain direct ideal answer [12].

The Manta ray forage optimal technique to enhance the dynamical functioning of grid-tied PV systems has been exemplified by the significant advancement of computer

algorithms and their effective use in tackling nonlinear objective functions. DC–DC and DC–AC converters were also commonly used throughout power electronics to manage the Voltage level of Photovoltaic panels for grid connection. Due to the apparent sensitivities of the solar PV towards the frequency of operation in the IV curves, the DC–DC charge controller is often used to track the maximum power output [5].

A nonlinear control model is implemented inside the PQ field that boosts the performance and availability of the suggested approaches within the grid-connected situation. Furthermore, a customized leader–follower agreement technique is implemented to organize other multi-functional grid-tied inverters to downscale adequate required power by the same factors that must create a place for the PQ operation. Unlike prevailing view approaches, which strive to guarantee that almost all individuals converge to the same condition for any beginning state, the methodologies seek to acquire the whole system's initial mode. Finally, the suggested upgrade option includes phase resolution [6].

As detailed above, several objective targets were presented throughout the previous for building the Solar panel and the DC–AC converter in a Photovoltaic system. However, the influence of the chosen optimization problem on the total PV system's electricity-generating efficiency is still not examined. To bridge that gap, this author conducted a comparison analysis, for perhaps the first time there in the available literature, to investigate the electricity production efficiency of PV systems wherein the Solar panel, as well as the DC–AC converters, were individually intended with different optimization technique utilizing multiple available optimization targets. Furthermore, the power generation of the Photovoltaic system created utilizing the suggested fundamental design approach represents the maximum limits of every Photovoltaic system's power generation capability. Consequently, the simulation results reported in this study were critical for assessing the efficacy as well as efficiency of the previous optimum design targets commonly used in developing the Photovoltaic system. As a result, this report provides practical advice for the proper design of Photovoltaic systems in energy production efficiency [7].

Two configurations of a residence are studied: PV panels and storage system, and PV panels and battery system. Real-world data spanning 10 years is used to maximize outcomes. Cash flows are calculated to show yearly payments. Descriptive analysis is done by changing system parts, power consumption, and retailing power prices. An example is a grid-tied residence in South Australia. The goal is to reduce payback time to under 10 years and maintain system viability. Two primary scenarios are considered: (1) selling back cost of energy equal to off-purchase cost, and (2) selling back cost of energy equal to original electricity cost taking into account technical and financial limitations.

The association seen between critical essential component fluctuation and the primary performance characteristics of a Photovoltaic panel depending on 8 important architectural parameters is shown [8].

To counter the impacts of amplified energy transfer between the MG and the utility's power allocation, the charging/discharging power of superconductive magnetic energy storage (SMES) and its voltage control power factor are evaluated simultaneously. The ideal superconducting magnetic energy storage charging/discharging volume is characterized by the ideal alteration in SMES current. To solve the modelling system while accounting for the limitations of the power grid, Voltage source converter, and SMES, a evolutionary algorithms approach, specifically particle swarm optimization, is employed.

When solar electricity production is insufficient, the fuel cell technology is used as a backup power supply but as an alternative to grid requirements. Furthermore, Lyapunov-approach inverter controllers with MPPT functionality through dc power management and high power factor operating at the PCC to grid utilities have been presented [9]. The fuzzy-based control system technique can reduce monitoring duration while simultaneously increasing precision [10].

A simulation software built upon that suggested controller was provided to be activated whenever connection speeds fell below a certain threshold. By synchronizing stages and spreading energy sources, this technology could help reduce the effect of Vehicle and scattered energy source variability [11]. Time-series estimation techniques, as well as Artificial Neural Networks, have been used to build statistical models. They offer an approach for obtaining the most sun radiation via a Photovoltaic panel instead of the most immediate electricity. The approach is known as optimized power point tracking, so it is built just on Perturb and Observe method principle [12].

A DVR with a fuzzy controller and phase adjustment was tested under fault scenarios such as faulty wiring and voltage sags. Real power restoration and minimal reactive power leakage are essential for data systems, and fast real power recovery is essential for frequency regulation in the power system. However, excessive active and reactive leakage can negatively affect voltage recovery and even lead to local voltage instability [13, 14]. The Simple Boost Control technique can increase the dc output. However, as Shoot-Through rises, the modulated signal lowers, causing a ripple voltage. These zero stages were employed because Shoot-Through stages in the Optimal Boost Control approach boost the dc output voltage. However, even though this approach reduces ripple voltage while increasing high gain, it causes low-frequency current fluctuations [15]. A single-stage photovoltaic system is preferred due to its advantages over a two-step process. It is connected to the power grid, load demand and voltage

control via a point of common coupling. The proposed Swarm optimization MPPT technique is an effective balance between installation convenience and accuracy in tracking the Global Maximum Power Point. This research will also assess the effectiveness of this special optimization method with microbial technique versus conventional MPPT algorithms in partial and dynamic shading scenarios.

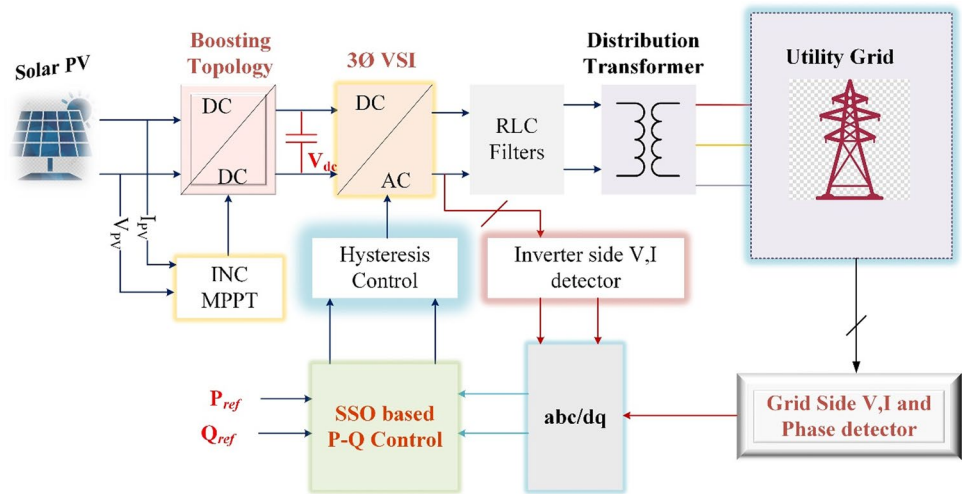
A recent investigation was conducted through a few different methods to manage the energy flow in Grids. The suggested technique utilizes P–Q control theory and hysteresis control through the utilization of Salp swarm optimization technique. To evaluate the technique, a 75 kW solar PV system with an inverter's real and reactive power capability was utilized. To begin with, the incremental conductance approach was used to attain adequate power. After this, the Salp swarm optimization strategy was used to control the inverters, and the results were compared to those of the Traditional feedforward controller, the PI controller, Genetic Algorithm (GA), and Particle Swarm Optimization (PSO) techniques. Out of these, SSO was found to be more favorable for this proposed research since it is highly adaptable and can solve a wide range of problems. Meta-heuristics reap the benefits of random operators since they fall under the umbrella of stochastic optimization methods. As real-life issues commonly have a large number of local optima, this helps them to reduce local solutions.

According to the literature review, the following are the list of the contribution of this study:

- It presents the Salp swarm optimization approach to increase a three-phase grid-connected photovoltaic system's reliability and power quality.
- Current Harmonic distortion is reduced and is compared to traditional approaches like PI, GA, and PSO when connected with grid PV systems.
- Using P–Q control theory to regulate the real and reactive power individually.
- In this study, several cases are discussed with various controllers and parameters in Sect. 4.

The body of the article is arranged as follows: The Overview of the System is described in Sect. 2 and discusses the model of a PV System, the MPPT technique with a DC–DC boost converter and solar PV Inverter Reactive Power Capabilities. Section 3 defines in detail the techniques of control for the Suggested System. Section 4 defines the suggested system's performance analysis under various cases with PI-based optimization controllers. Section 5 contains a full explanation of real-time implementation and its performance analysis. And thus, results and discussions of the proposed technique are examined. Eventually, Sect. 6 concludes the article.

Fig. 1 Proposed configuration with SPV architecture



2 Overview of the System

The suggested architecture of the three-phase Grid-integrated PV system is depicted in Fig. 1. Solar energy systems, Chopper, Maximum Power Point, inverters, filters, and distributed generation are all part of it. A DC–DC power converter outputs circuit maintains the DC link voltage. The generated output from Photovoltaic panels is used as a source to a boost converter, which then delivers continuous power towards the DC-Link. An incremental conductance approach could be employed to collect the high power from PV. Eventually, the alternating current is generated using a VSC using a hysteresis controller. A serial RL and a shunt RC network combination deliver high-quality outputs with the required frequencies and voltages. The output terminals of the inverters are linked to the transmission system, which transmits electricity to the utility grid. IEEE33 bus distribution system is utilized in the electric grid to validate the results.

2.1 Model of a PV System

The structure of the Photovoltaic system is critical in achieving excellent efficiency and quality from solar PV. The input current is shunted using a diode in the photovoltaic, as well as the output is sworn mainly through the cell’s solar beams. To achieve the fundamental superiority need, a number of parameters could be coupled in parallel or series [5]. Table 1 lists the simulated settings for the Photovoltaic panel.

2.2 MPPT Technique with a DC–DC Boost Converter

Utilizing 50 parallel threads and 5 serial strings, the chosen Solar panel generates 75 kW of maximum electricity. Figure 2 illustrates the Solar PV system’s performance curves

Table 1 PV module designing parameters

Sun power SPR-306E–WHT-U	
Maximum power	315.117 W
Open circuit voltage	63.89 V
Short circuit current	6.01 A
Voltage at MPP	55.1 V
Current at MPP	5.88 A
Cells per module	94
Number of parallel strings	48
Number of series strings	6

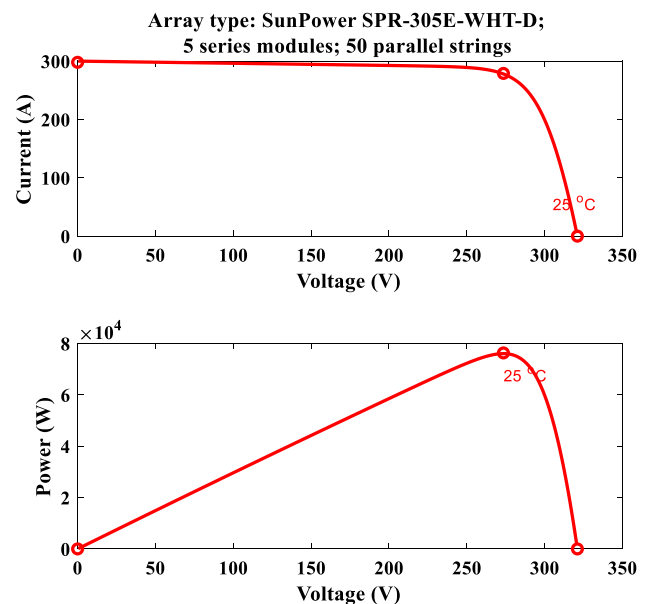


Fig. 2 Solar PV curve

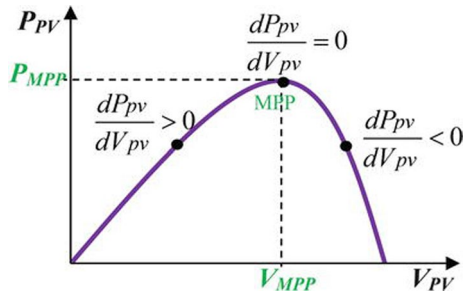


Fig. 3 Characteristics curve of P–V by INC technique

under the ambient condition and irradiance settings. Environmental conditions are influencing the maximum power of photovoltaic Systems. The Incremental conductance structure is used to harvest the highest power from the sun while it is partially shaded. MPPT is used to discover the variability in climatic variations to achieve optimum distribution after the PV. Figure 3 depicts P–V characteristics as determined by the INC technique. Precise control is occurring, including moderate perturbation states. The duty cycle D of the power converter is adjusted to ensure the Voltage level that provides constant power to the inverters. The duty ratio varies depending on the specific weather conditions. The formula for boost converter’s system requirements in Eq. (1) [5].

$$L = \frac{V_{vos}D}{2\Delta_j f_{sf}} \tag{1}$$

where D = duty ratio and is stated as,

$$D = 1 - \left(\frac{V_{in}}{V_{out}} \right) \text{ and } V_{vos} = \text{Voltage output of the solar cell.}$$

Δ_j is ripple current output and f_{sf} is the switching frequency of the converter [5].

2.3 Solar PV Inverter Reactive Power Capabilities

Real power is helpful throughout the electricity transmission industry, but reactive power is unneeded since that boosts power dissipation and load current and affects the overall power management. The angle between real and apparent power is the power factor (θ); the power factor changes depending on the inductive load connection. As a result, the power factor is crucial in coupling an inductive load that accomplishes the utility’s reactive power requirements. In addition, the grid voltage pattern is influenced by reactive power usage. Therefore, reactive power must be supplied in a controlling way to boost grid voltage levels. Traditionally, capacitors are often utilized to supply reactive power into the system to keep it steady.

Grid-connected PV inverters are already being suggested to supply reactive electricity efficiently. The

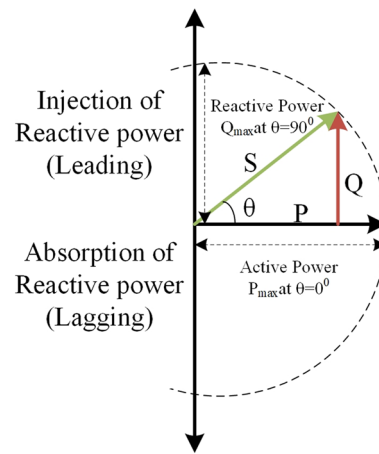


Fig. 4 PV inverter operations across two quadrant

inverters may operate in both positively reactive and negatively reactive modes, providing reactive power and reducing voltage stability. Figure 4 exposes the inverter’s reactive power capability, with the real, reactive, as well as apparent power of an inverter designated as P , Q , and S . The power factor of the network is determined by the angle θ ; when $\theta = 0^\circ$, reactive power was nil, as well as the inverters, provide active power ($S = P_{max}$), when $\theta = 90^\circ$, the inverters may ultimately provide reactive power with nil active power ($S = Q_{max}$).

The amplitude, as well as the angles of a PWM inverter, are varied to manage reactive power. The Voltage source inverter’s quadrature axes current manages reactive power outputs. The inverter is significant because it is like STATCOM and can perform in VAR modes with little disturbance. The inverters might also provide or absorb reactive power by adjusting the quadrature axes’ current.

3 Control Techniques for the Suggested System

3.1 Methodology for Controlling Inverters

The inverter controller for power factor correction is quite tricky owing to system constraints. To examine the harmonics distortions, every phase must be individually regulated during design, as well as the system’s momentary circumstances should grow increasingly complicated. The algebraic translation of the three-phase vectors abc into the two-phase vectors dq overwhelms such complexities. During stable circumstances, signals are represented as a single direction in dq conversion. Distractions of the utility grid seem to affect that dq transformation. As a

result, this technique may help assess grid-tied systems. The Phase-Locked Loop is used to synchronize grid voltage levels and phase differences. Combining the angular reference frequencies yields the reference angles. The phase angle ωt of the PLL is employed to transform the variables abc into dq. Formulae (2) and (3) are used to translate the observed grid currents and voltages together into a reference frame,

$$\begin{bmatrix} V_{gd} \\ V_{gq} \\ V_{g0} \end{bmatrix} = \sqrt{\frac{2}{3}} \begin{bmatrix} \sin P & \sin Q & \sin R \\ \cos P & \cos Q & \cos R \\ \frac{1}{\sqrt{2}} & \frac{1}{\sqrt{2}} & \frac{1}{\sqrt{2}} \end{bmatrix} \begin{bmatrix} V_{ga} \\ V_{gb} \\ V_{gc} \end{bmatrix} \tag{2}$$

$$\begin{bmatrix} i_{gd} \\ i_{gq} \\ i_{g0} \end{bmatrix} = \sqrt{\frac{2}{3}} \begin{bmatrix} \sin P & \sin Q & \sin R \\ \cos P & \cos Q & \cos R \\ \frac{1}{\sqrt{2}} & \frac{1}{\sqrt{2}} & \frac{1}{\sqrt{2}} \end{bmatrix} \begin{bmatrix} I_{ga} \\ I_{gb} \\ I_{gc} \end{bmatrix} \tag{3}$$

wherein, $P = \omega t$, $Q = \omega t - \frac{2\pi}{3}$, $R = \omega t + \frac{2\pi}{3}$, V_{gd} , V_{gq} , i_{gd} , i_{gq} seem to be the dq vector voltages and currents, and V_{ga} , V_{gb} , V_{gc} , I_{ga} , I_{gb} , I_{gc} seem to be the three-phase grid voltages and currents, respectively. The innermost loops of an inverter in the suggested Salp swarm optimization technique operate using dq dimensions in DC unbalanced systems. The suggested controller generates the V^{abc} by delivering the real reference voltages V_d^* and the reactive reference voltages V_q^* , which are then transferred towards the hysteresis controller, which generates the inverter’s gating signals. The decoupling P–Q theories differentiate real and reactive currents in the inner loop.s Fig. 5 displays the grid-connected

solar inverter’s decoupled P–Q controller. Equations (4) and (5) are used to calculate the active and reactive power with Park’s transformation.

$$P = 1.5(V^{od} * i^{od} + V^{oq} * i^{oq}) \tag{4}$$

$$Q = 1.5(V^{od} * i^{od} - V^{oq} * i^{oq}) \tag{5}$$

wherein V^{od} , i^{od} , V^{oq} , i^{oq} represent the dq grid currents and voltages. As a result, the suggested inner loop Salp swarm optimization approach correctly tracks current signals and avoids short-circuit current nonlinearities. In addition, a hysteresis voltages control has now been introduced to increase power accuracy and reduce the grid’s current harmonic distortion.

3.2 Voltage Hysteresis Controller

Complex scenarios impact the power quality of a power system. Because of its durability, rapid fault tracking capabilities, superior transient characteristics, and simplicity of implementation over traditional controllers, a hysteresis voltage controller is created to increase Grid Stability in dynamic settings. As a result, the suggested real reference voltages V_d^* and reactive reference voltage V_q^* generate the I_{abc} , which is then passed towards the hysteresis controller, which generates the inverter’s gating signals. Consequently, the hysteresis spectrum is created with a desire based on the Δv -error value of the actual and reference voltages of the grids. If the Δ error exceeds the higher spectral levels,

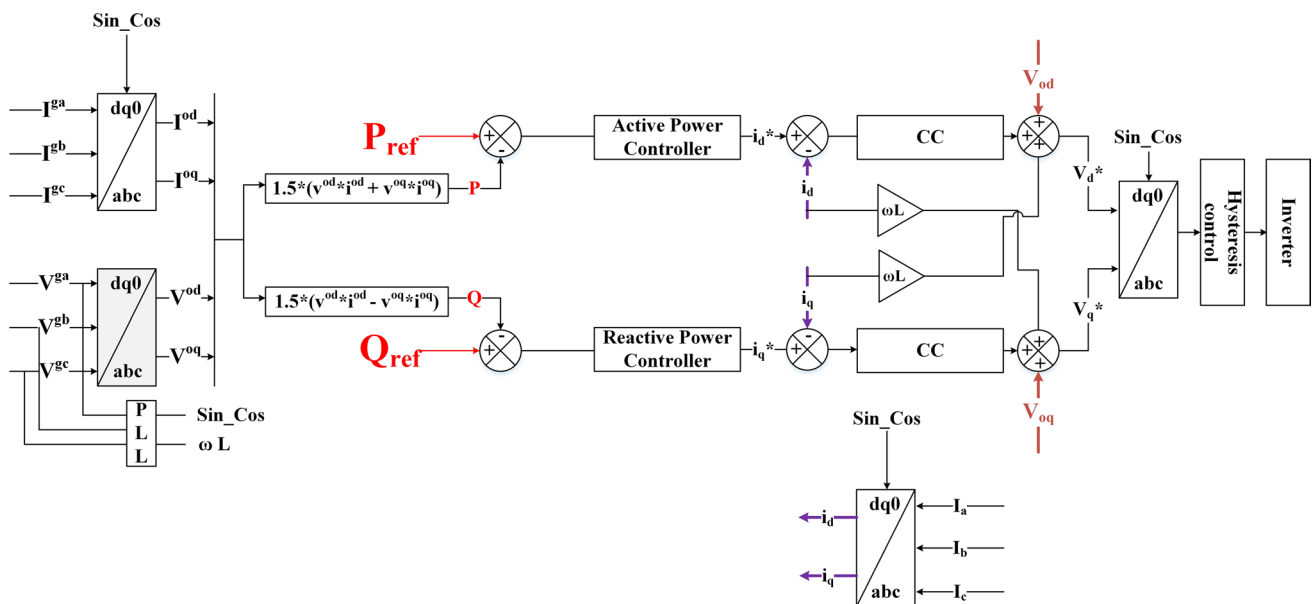


Fig. 5 P–Q control for grid-connected PV inverters

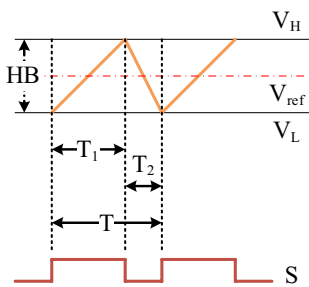


Fig. 6 Hysteresis band voltage control

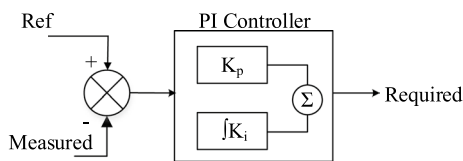


Fig. 7 Structure of mathematical PI controller

the lower-level switches of the inverters are activated; conversely, if Δ the error gets to lower band values, the upper-level switches of the inverters are activated. Figure 6 depicts the inverter’s hysteresis band voltage control. Equations (6) and (7) are used to determine the link between the inverter’s operating frequency, hysteresis band, and Harmonic distortion.

$$a_1 + a_2 = a_c = 1/f_c \tag{6}$$

$$THD(\%) = \left(\left(\sqrt{\sum_i^m v_i} / v_1 \right) \times 100 \right) \tag{7}$$

3.3 Real and Reactive Power Control

A grid’s functionality depends upon the injection/absorption of active and reactive power. Real and reference power are sent into the computational PI controller to provide an effective outcome in grid connection. In contrast, the PI controller is unsuitable for dynamic load situations. As a result, this paper offers a Salp swarm optimization approach for controlling reactive power injections in the grids under dynamic loading and steady-state settings.

3.4 Structure of Mathematical PI Controller

The real and reactive power on the grid is monitored using sensing equipment and sent into the comparator blocks. The

comparator then measures the average and reference power and sends the results to the controllers to generate switching pulses. Ultimately, the controller provides the necessary power during injection and absorption. Figure 7 depicts the Conventional Mathematical Structure of PI Controller.

Only under steady-state conditions does the computational PI controller provide enough power. Furthermore, the PI controller gains parameters were determined through numerical techniques of a fairly complex system. This paper proposes Salp swarm optimization to eliminate those problems.

3.5 Genetic Algorithm-Based PI Controller

An optimization technique would be a form of full search that can be used to resolve complex variables and optimize difficult tasks. GA employs randomized transition rules rather than predictable principles and repeatedly evolves a community of reasonable options called chromosomes. A generation is indeed the name given to every other algorithm step. Steps like reproduction, crossover, and mutation are used to mimic the development of systems. As shown, an optimization algorithm is often started with a population of individuals. Chromosomes, a genuine binary string, often express each population. The fitness function measures and assesses an individual’s knowledge by assigning every individual a corresponding number known as its performance. Every chromosome’s viability is evaluated, and a selection of the fittest technique is used. The error signal is employed in this study that estimates every chromosome’s fitness. An evolutionary algorithm has three major operations: reproduction, crossover, and mutation [16].

Stage 1: Set the parameters using a set of random values, like the crossover probability, number of iterations, number of nodes, and reproduction numbers. Decide on the code method.

Stage 2: Calculate and assess the fitness function’s values.

Stage 3: Continue with said mutation and crossover operations to implement the entire clusters.

Stage 4: Steps 2 and 3 should be repeated until the optimum values are attained.

PI Optimization Using a Genetic Algorithm is discussed in the following section. GA creates a randomized population initially, which is then applied with a modest population sufficient to accommodate the controllers ever to be tuned and convergence at a quicker pace. Transforming the PI parameters K_c , T_i , and T_d in binary representation called chromosomes yields the starting population. Every chromosome’s viability is computed by translating its binary text into an actual number that specifies the PI parameters. The PI controller receives every pair of PI parameters. Respective

Table 2 GA parameters utilized in the simulations

Parameters	Values/ranges
Maximum generations	115
Encoding	Binary
Population size	22
Crossover	One point
Mutation	Uniform
Selection	Uniform

cost measures such as ISE, IAE, and ITAE and a weighting mixture of such 3 cost functions are used to estimate the system’s total reaction for every PI parameter and its starting transfer function. This procedure will repeat Stages 2 and 3 until the highest fitness level is attained at the generation’s conclusion. The main goal of GA is to find global PI parameters (K_c , T_I) with the lowest optimal solution for operating the plants across the entire array. Table 2 shows the specifics of the GA parameters utilized in the simulations.

3.6 Particle Swarm Optimization-Based PI Controller

PSO is modelled on the swarming behaviour of bird groups when looking for food. To modify the locations of the particulate, the method collects inputs from the local and global cheapest options. As a result, the particles were predicted to travel to sites near optimum spots. Figure 8 depicts the PSO flowchart for solving the optimum inverter solution.

Finally, the positional adjustment method is carried out in each repetition using the mathematical equation:

$$P_{sd} = (w * P_{sd})l_1 * random\ number * (local\ finest - P_{dr}) + l_2 * random\ number * (global\ finest - P_{dr}) \tag{8}$$

In Eq. (8), l_1 and l_2 are the training variables, while P_{sd} and P_{dr} are still the particle’s speed and direction, accordingly. As previously indicated, the speed is updated using the optimum local and global parameters. Accordingly, those are known as the “local finest” and the “global finest”, accordingly. Upon determining the speeds, the positions are easily adjusted using the linear formulas: [17]

$$P_{sd} = P_{sd} + P_{dr} \tag{9}$$

The following are the steps of the Particle swarm approach for solving the optimal inverters solution:

Stage 1: The initiation stage selects the system configuration and initializes the particles. The particles as well as the training parameters l_1 and l_2 are indeed the factors considered. Depending on the severity of the inverter being researched, every particle comprises three, five, or seven

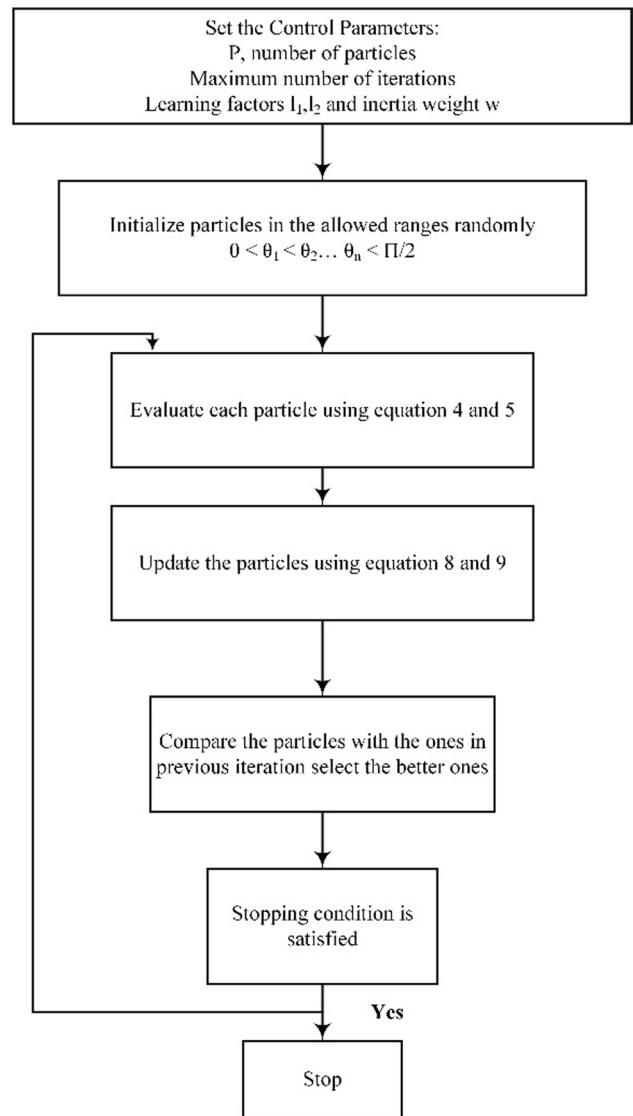


Fig. 8 PSO flowchart

values. As a result, the constituents of every particle must incorporate the standard condition: $0 \leq \theta \leq \pi/2$.

Stage 2: To determine the model parameters of every particle, the finest local and global objectives are then identified.

Stage 3: By equation, the particles’ speeds were adjusted using training variables and the local and global optimum results (8). Finally, an equation is used to modify the positions (9).

Stage 4: Evaluate the upgraded components and their related switching orientations of the proposed grid-tied inverter. The findings are presented in the following iteration’s outcomes: the more particles kept, the finer.

Stage 5: The finest values on a local and global scale are upgraded.

Stage 6: This phase determines whether the algorithm should be stopped or continued. The halting condition typically examines for achieving the iteration number or analyzes the quantitative disparities between the best optimally acquired so far and those achieved I iteration earlier. Whereas if the choice is to halt, the algorithms produce the phase angle; alternatively, it returns to the third phase [17].

3.7 Salp Swarm Optimization (SSO)

In the optimization procedure, SSO mimics the swarm behaviour of salps. Salps construct salp networks to improve their mobility ability and simplify access to the food supply. Like other heuristic approaches, Viable alternatives are more critical in getting remedies. As a result, the finest Salp, known as the chain’s main Salp, is emulated by several others. For example, Salp’s goal is to go to the food supply or the best answer. Figure 9 depicts the flowchart of the execution of the SSO to the inverter’s optimum solution. As a result, at the end of the procedure, every individual in the Salp community was predicted to migrate towards the optimum alternative.

Positioning modifications of the primary salps and followers are carried out using Eqs. (10) and (12) shown below [18].

$$y_i^1 = \begin{cases} G_i + d_1(ub_i - lb_i)d_2 + lb_id_3 \geq 0 \\ G_i - d_1(ub_i - lb_i)d_2 + lb_id_3 \geq 0 \end{cases} \quad (10)$$

wherein y_i^1 is the leading Salp, G_i is the positioning of the food supply, ub_i as well as lb_i were top and bottom bounds, and d_1, d_2 , and d_3 are randomized integers. The following is the definition of variable d_1 [18]:

$$d_1 = 2e^{-\left(\frac{l}{L}\right)^2} \quad (11)$$

wherein l and L denote the present number of iterations and the maximum number of iterations number, respectively. Finally, the location of the follower’s salps is updated using Newton’s law of motion [18]:

$$y_i^1 = \frac{1}{2}V_p t^2 + V_0 t \quad (12)$$

In this case, V_0 represents the starting speed, and V_p is determined by dividing the end speed by the actual speed.

The following are the steps of the SSO approach for solving the optimal inverter solution: [18]

Stage 1: The salps are activated at this stage. Every Salp entry correlates toward a shifting angle. Variables are initialized at randomized within the permitted integer values. In other terms, the number of salps is N_s , and each Salp is made up of s components that vary from 0 to $\pi/2$ that

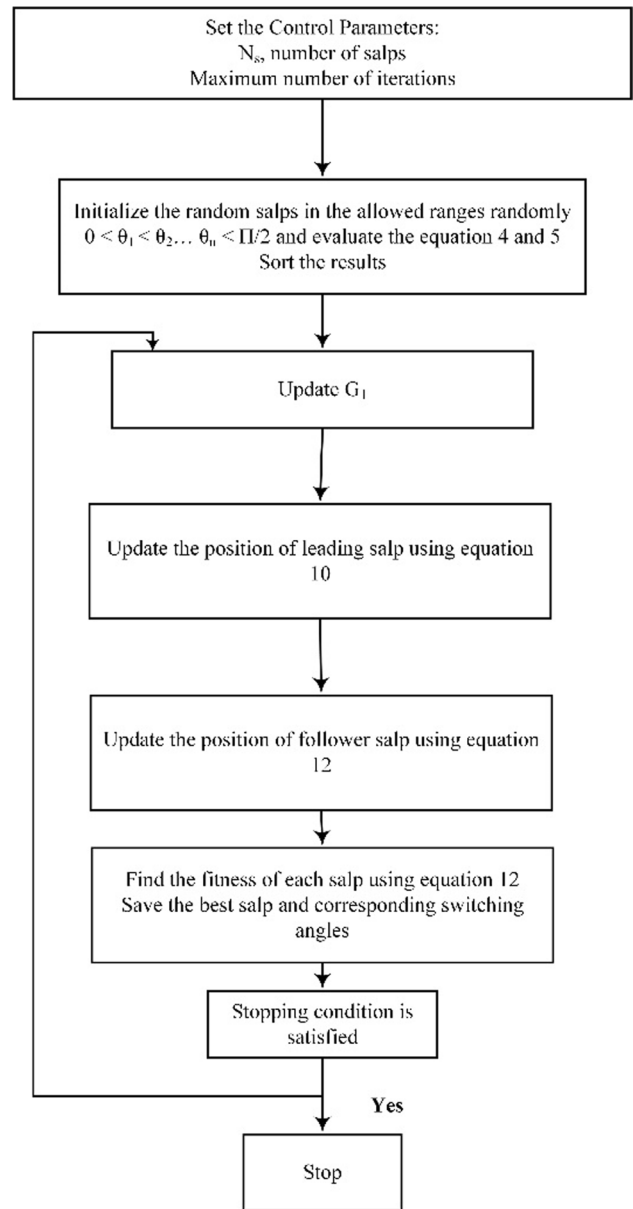


Fig. 9 Flowchart of the execution of the SSO

meet the condition: $0 \leq \theta \leq \pi/2$. For Inverters, the number of parameters in every Salp would change.

Stage 2: The entries of every Salp were fed into an inverter, as well as the optimal solution of each Salp was computed.

Stage 3: The real solution among the solutions contenders is the leader. It’s also discovered through grouping the salps based on the outcomes of the optimal solution assessments. The other alternatives, or followers, are supposed to obey the leader. Equations (10) and (11) are used to modify the leader’s location.

Stage 4: Equation (12) modifies the followers’ locations.

Stage 5: This stage identifies whether the approach should be stopped or continued. It either compares the variances between the best approaches after predetermined iterations else compares the optimal solution. If the algorithm doesn't really come to a halt, it proceeds to stage 2.

4 Suggested System's Performance Analysis

A 75 kW Grid-tied PV inverter is considered in this work for reactive power and current Harmonic distortion control. The Matlab Simulink environment is utilized to validate the proposed system's results. Solar PV, DC–DC Power converter, Hysteresis Controllers VSC, and IEEE 33 distribution serve as a power system in the developed framework. Derived solar electricity is supplied into the incremental conductance Maximum PowerPoint that offers the most power in various environmental situations. Photovoltaic power is increased with a boosting topology to sustain the DC supply and improve the system's stability. VSC is controlled using integrated P–Q theories and a hysteresis controller. Eventually, DC/DC converter is linked towards the power transformer through a filtering circuit to provide continuous outputs. Real and reactive power are individually managed using different controllers in this suggested research. The researchers of [4] disclose the power quality analysis using the feedforward controllers. Three distinct controllers are implemented in this research that analyzes and evaluate the proposed one.

Several scenarios with distinct controllers and characteristics are explored in this paper.

- Harmonic current distortion study with reactive power injection and absorption using various controllers.
- Harmonic current distortion study using various controllers at unity power factor.
- Harmonic current distortion study using just reactive power assuming SPV power is not present.
- Harmonic current distortion study considering different irradiances using various controllers.
- Analyzing the operation of controllers.

4.1 Case A: Current Harmonic Distortion Study with Reactive Power Injection and Absorption Using Various Controllers

The reference value controls the injection and absorption of reactive power independently. Real power is kept consistent throughout this situation, while reactive power absorption (Q-Negative) varies with random values; distinct controllers manage the real and reactive power. Consequently, assuming

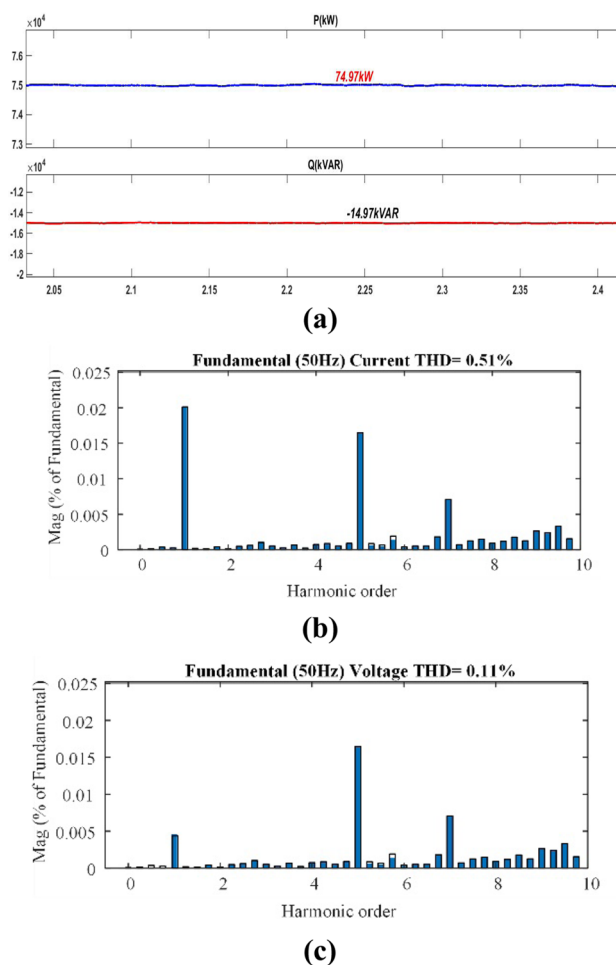


Fig. 10 Results of simulation involving reactive power absorption at a reference 15kVAR for the proposed system, **a** real and reactive power, **b** current harmonic distortion, **c** voltage harmonic distortion

constant real power, a reference point of reactive power is adjusted between 75 and 15 kVAR. The feedforward controller controls reactive power, and the present Total harmonic current distortion is 5.46 percent under the 15kVAR reference. Decoupled P–Q theories using a PI controller decrease current harmonic distortion and optimize power. The current harmonic distortion at 15kVAR reference power is 3.47 percent. Eventually, Salp swarm optimization is used in P–Q theories to achieve exact results.

Consequently, the reference voltage is 15kVAR; the current harmonic distortion is 0.51 percent, and the voltage harmonic distortion is 0.11 percent, with the real power remaining at 75 kW. Figure 10 depicts the simulation findings for reactive power retention. Table 3 additionally shows the investigation results utilizing controller design for various reference values.

Table 3 Absorption of reactive power (Q-negative) with different types of controllers

Q Ref	Absorption of reactive power (Q-negative)																								
	Feed forward methodology			PI controller			PSO based controller			GA based controller			SSO based controller												
	P	Q	SPV	V	THD	I	P	Q	SPV	V	THD	I	P	Q	SPV	V	THD	I							
75	67.13	-67.72	75.34	0.33	2.79	66.42	-65.62	76.1	0.24	2.51	71.27	-71.47	76.2	0.24	1.97	73.57	-73.05	75.98	0.21	0.62	74.97	-74.97	75.14	0.11	0.29
60	67.46	-51.78	75.45	0.33	3.98	66.43	-50.24	76.15	0.24	2.68	71.54	-57.32	76.21	0.24	2.13	73.24	-58.24	75.92	0.21	0.86	74.98	-60.01	75.14	0.11	0.37
37.5	67.69	-32.29	75.66	0.33	4.25	66.57	-31.97	76.15	0.25	3.12	72.3	-33.58	76.15	0.25	2.98	74.52	-35.12	75.92	0.19	0.92	75.01	-37.24	75.14	0.11	0.48
15	67.98	-13.8	75.8	0.34	5.46	66.48	-12.1	76.12	0.27	3.47	72.37	-13.67	76.15	0.27	3.17	74.51	-13.58	75.88	0.19	1.13	75.2	-14.97	75.14	0.11	0.51

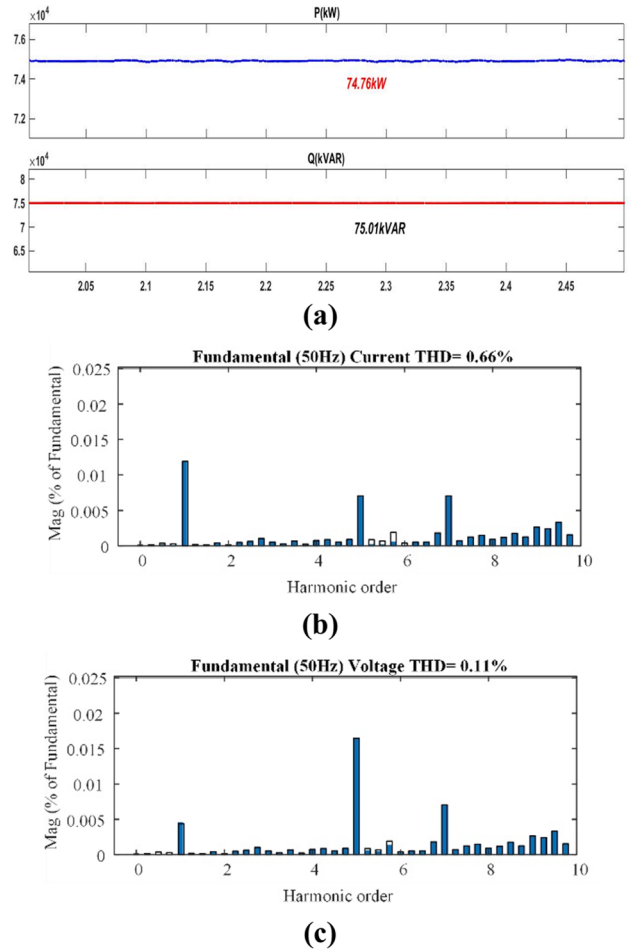


Fig. 11 Results of simulation involving reactive power injection at a reference 75kVAR for the proposed system **a** real and reactive power, **b** current harmonic distortion, **c** voltage harmonic distortion

The same scheme is used for the system with reactive power injection (Q-Positive). In the reactive power injection modes, current harmonic distortion in feedforward methods of control is 5.04 percent at 75 kVAR of references. Using this proposed model, the existing Harmonic distortion result is lowered to 3.27 percent at 75 kVAR of references. Consequently, there is no discernible difference in voltage Harmonic distortion between the injection and absorption stages. Figure 11 depicts the results of the reactive power injection using simulation. Table 4 illustrates the results of the data study using different controllers with various reference settings. Figure 12 depicts a pictorial representation of reactive power absorption and injection. According to the analysis, the suggested system’s current harmonic distortion is within the threshold point of 0.66 percent in various operating modes. Figure 13 depicts the current Harmonic distortion overview of the available controllers and reference values using reactive power injection and absorption.

Table 4 Injection of reactive power (Q-positive) with different types of controllers

Injection of reactive power (Q-positive)		Feed forward methodology					PI controller					PSO based controller					GA based controller					SSO based controller				
Q Ref		P	Q	SPV	V THD	I THD	P	Q	SPV	V THD	I THD	P	Q	SPV	V THD	I THD	P	Q	SPV	V THD	I THD	P	Q	SPV	V THD	I THD
-75		67.58	65.5	75.99	0.35	5.07	67.52	64.32	76.21	0.26	3.27	71.58	69.27	75.69	0.26	2.17	74.04	71.02	75.2	0.26	1.71	74.76	75.01	75.41	0.12	0.66
-60		67.66	52.44	75.98	0.35	5.23	67.56	51.27	76.12	0.28	3.87	72.04	53.62	75.68	0.25	2.67	74.12	56.19	75.4	0.25	1.86	74.78	59.98	75.27	0.12	0.79
-37.5		68.17	33.01	75.94	0.35	5.46	68.02	30.98	76.34	0.27	4.12	72.54	34.28	75.67	0.25	3.12	74.25	36.12	75.4	0.25	2.12	74.89	37.51	75.46	0.11	0.72
-15		68.03	13.36	75.87	0.34	5.54	68.17	11.57	76.14	0.27	4.58	72.58	13.67	75.61	0.24	3.16	74.25	14.21	75.4	0.24	2.47	74.89	15.03	75.87	0.11	0.86

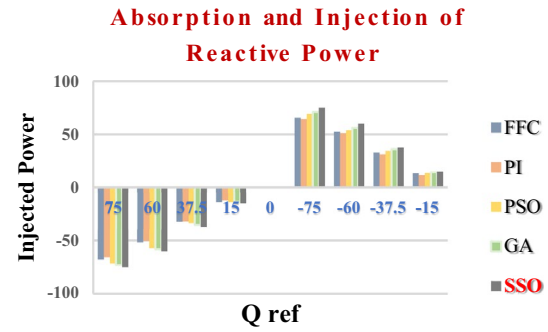


Fig. 12 Comparison of controller performances during reactive power injection and absorption

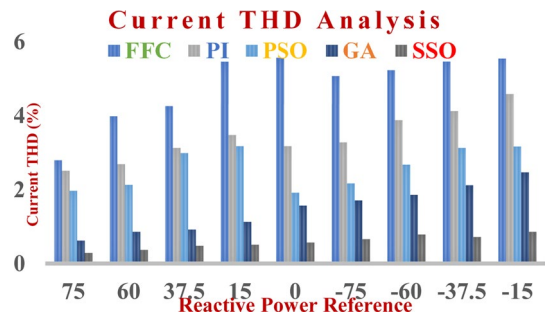


Fig. 13 Current Harmonic distortion comparison of several controllers and reference values

4.2 Case B: Harmonic Distortion Study Using Various Controllers at the Unity Power Factor

In achieving a UPF condition, the inverters must supply a maximum of real power while using zero reactive power flow. UPF conditions real power is 69.76 kW and reactive power is 0.75 kVAR with a current Harmonic distortion of 5.56 percent in the traditional feedforward approach.

In decoupled P–Q theories with a Proportional gain controller, real power equals 75.14 kW with a current Harmonic distortion of 1.57 percent. Moreover, a Salp swarm optimization generates additional real power with the least current Harmonic distortion. Consequently, the maximal real power is 75.02 kW, and the reactive power is 0.0254kVAR, with a current Harmonic distortion of 0.57 percent, as shown in Fig. 14. As a result, the research stated that the present THD is somewhat greater than reactive power control and absorption. Table 5 depicts the results of an analysis of several controllers under UPF conditions.

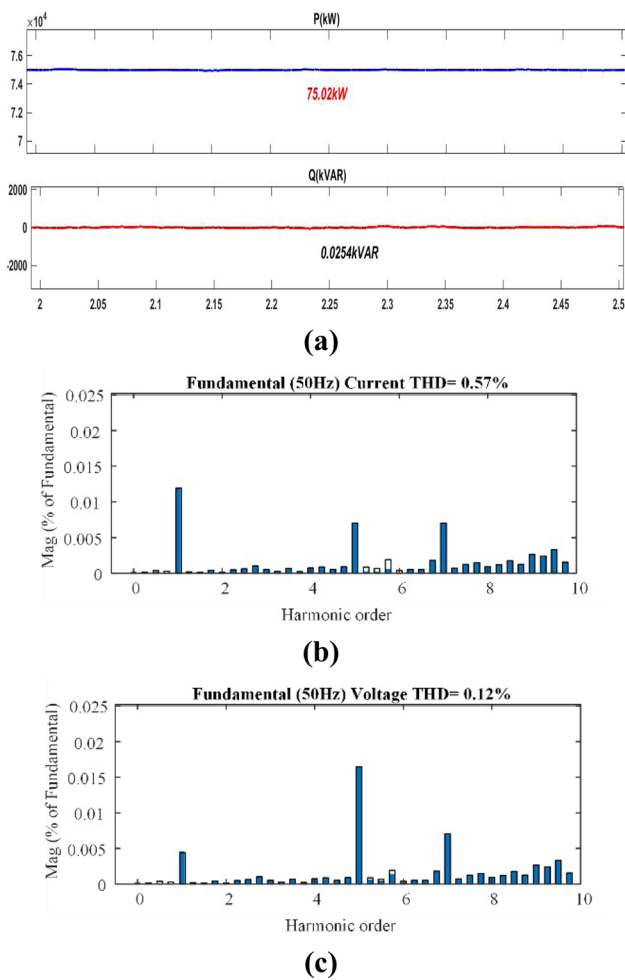


Fig. 14 Results of a simulation of UPF case **a** real and reactive power, **b** current harmonic distortion **c** voltage harmonic distortion

4.3 Case C: Harmonic Distortion Study Using Just Reactive Power, Assuming SPV Power is Not Present

Renewable energy varies according to environmental circumstances. For instance, solar power is inaccessible at nighttime. Therefore, reactive power is required at nighttime to control the grid. In this research, the inverters may operate as a STATCOM during the night to give reactive power from the grid and retain voltage control. The night mode scenario inverters in the traditional feedforward technique provide a great reactive power of 10.63 kVAR with a current Harmonic distortion of 13.9 percent at 15 kVAR of reactive power references. Decoupled P–Q theory is used in conjunction with different controllers to reduce Harmonic distortion and regulate electricity in the grid system.

Consequently, Salp swarm optimization produces a peak reactive power of 14.95 kVAR with a current

Table 5 Peak real power injection with different types of controllers

Q Ref	Unity power factor																								
	Feed forward methodology			PI controller			PSO based controller			GA based controller			SSO based controller												
	P	Q	THD	V	I	THD	P	Q	THD	SPV	V	I	THD	P	Q	THD	SPV	V	I	THD					
0	67.96	0.75	76.86	1.14	5.56	66.54	0.57	76.52	0.47	3.17	74.27	0.357	75.21	0.27	1.92	74.97	0.14	75.14	0.24	1.57	75.02	0.0254	75.57	0.12	0.57

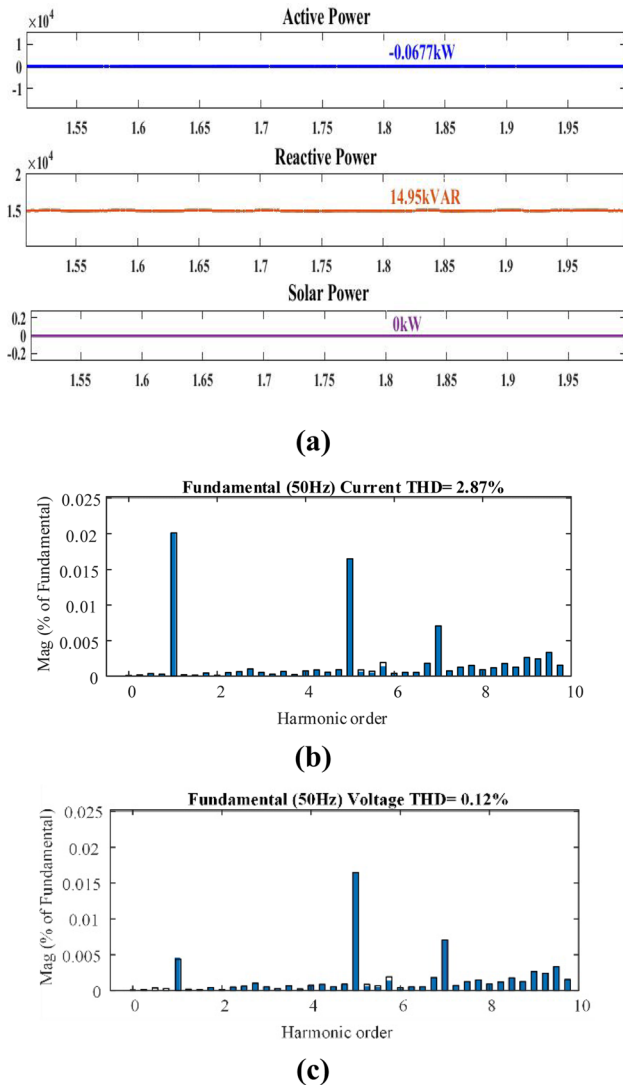


Fig. 15 Results of a simulation involving an absence of SPV case **a** real and reactive power, **b** current harmonic distortion, **c** voltage harmonic distortion

Harmonic distortion of 2.87 percent for 15 kVAR references, as shown in Fig. 15. Table 6 depicts a comparison of several controllers in night vision. As a result, the PV inverter could produce significant electricity at night to preserve grid control.

4.4 Case D Harmonic Distortion Study Considering Different Irradiations Using Various Controllers

Irradiations are modulated at a specified temperature using different control strategies to monitor the efficiency of photovoltaic panels. Solar Photovoltaic irradiance, for instance, is changed between 1000 and 200 W/m² at a fixed temperature of 25°. Consequently, the system can provide 13.15 kW of active power using the feedforward

Table 6 Night mode operation with different types of controllers

Q Ref	Night mode (no active power) irradiation = 0																								
	Feed forward methodology					PI controller					PSO based controller					GA based controller					SSO based controller				
	P	Q	SPV	V	I THD	P	Q	SPV	V	I THD	P	Q	SPV	V	I THD	P	Q	SPV	V	I THD	P	Q	SPV	V	I THD
75	-1.814	66.22	0	1.15	5.04	-0.914	67.54	0	0.16	3.14	-0.74	69.8	0	0.14	1.74	-0.31	71.02	0	0.15	1.12	-0.0143	75	0	0.11	0.53
60	-1.385	50.21	0	1.15	5.69	-0.585	51.21	0	0.18	3.99	-0.57	53.28	0	0.14	3.96	-0.36	56.19	0	0.14	2.84	-0.0234	59.99	0	0.11	0.68
37.5	-1.51	30.67	0	1.14	10.7	-0.71	30.47	0	0.18	9.7	-0.49	35.94	0	0.14	7.64	-0.27	36.12	0	0.14	4.5	-0.0571	37.48	0	0.12	1.13
15	-1.653	10.63	0	1.14	18.88	-0.853	10.57	0	0.18	15.78	-0.37	13.71	0	0.13	9.7	-0.23	14.21	0	0.13	5.14	-0.0677	14.95	0	0.12	2.87

Table 7 Solar irradiation variation for different controllers

Irradiation		Different solar irradiances with constant temperature																							
		Feed forward methodology			PI controller			PSO based controller			GA based controller			SSO based controller											
P	Q	SPV	V	I	THD	P	Q	SPV	V	I	THD	P	Q	SPV	V	I	THD	P	Q	SPV	V	I	THD		
1000	67.96	0.252	75.86	0.14	3.56	71.57	0.357	75.71	0.14	3.12	74.67	0.147	75.97	0.13	2.37	75.04	0.126	75.67	0.13	2.21	75.01	0.03291	75.75	0.12	0.48
800	54.68	0.452	60.63	0.14	5.27	56.78	0.362	59.85	0.14	4.85	58.41	0.246	60.54	0.13	2.85	58.97	0.174	60.19	0.13	3.14	60.19	0.00238	60.69	0.12	1.14
600	41.2	0.395	45.29	0.14	6.29	41.98	0.378	46.12	0.14	6.24	43.98	0.415	45.68	0.11	5.14	43.87	0.041	45.27	0.13	5.92	44.99	-0.006	45.31	0.11	2.64
200	13.15	-0.393	14.64	0.14	17.82	13.97	-0.314	13.25	0.14	11.57	14.17	-0.217	15.01	0.11	8.96	14.69	-0.119	15.01	0.11	6.18	14.26	-0.0012	14.41	0.11	3.64

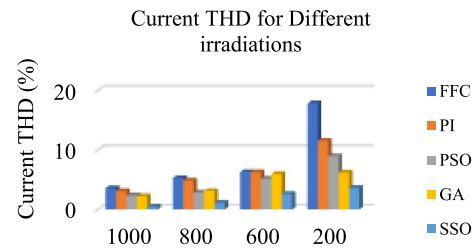


Fig. 16 Controller performance during solar irradiation variations

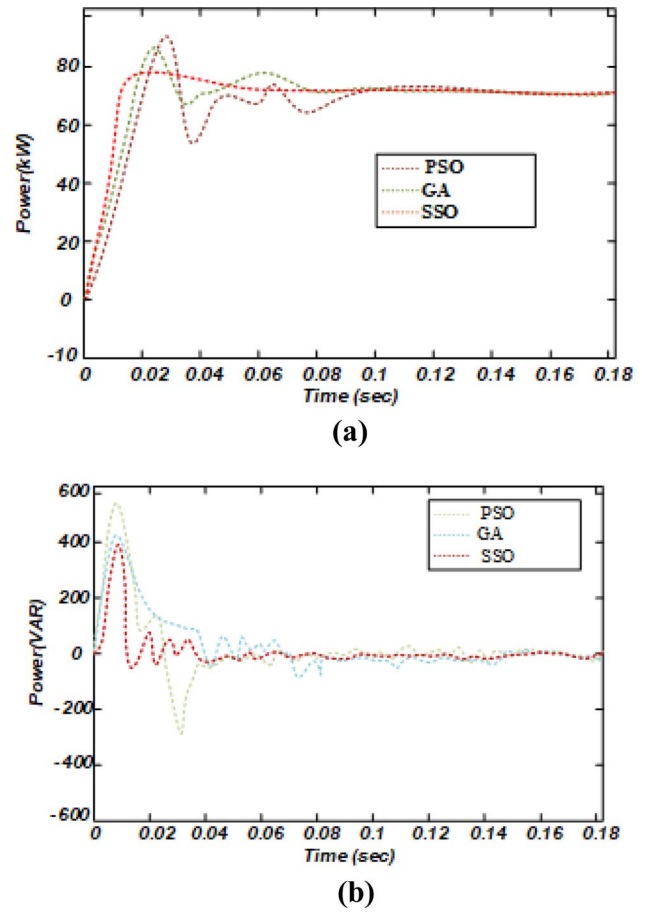


Fig. 17 Performance evaluation of various controllers **a** Active power, **b** reactive power

methodological approaches with 17.82 percent current Harmonic distortion at 200 W/m² of solar irradiation. As a result, the precise quantity of irradiance in the proposed approach yields 14.26 kW of real power with a THD of 3.64 percent. Table 7 presents a performance study of varying solar irradiance with various controllers. In addition, Fig. 16 depicts a graphical depiction of solar irradiation and current Harmonic distortion of various controllers.

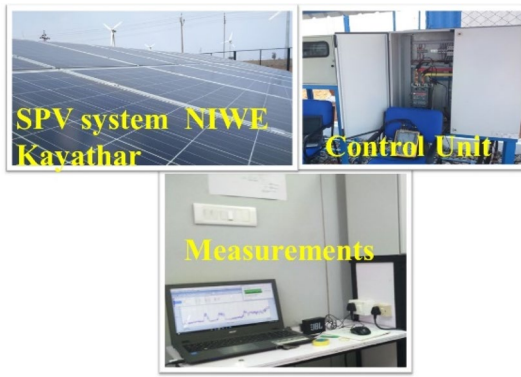


Fig. 18 Prototype model of grid-tied PV inverter

4.5 Case E: Analyzing the Operation of Controllers

The robustness of every controller has been evaluated in this scenario. The investigation was applied in the Unity Power Factor situation with inverters reference standards $P=75\text{ kW}$ and $Q=0\text{ kVAR}$. Logical PI controllers, GA, PSO, and Salp swarm optimization controllers are presented to create real and reactive power in decoupled P–Q theories. The power production of various controllers is depicted in Fig. 17. Salp swarm optimization yields improved outcomes with less overshooting, a settling time of 0.04 ms, as well as a slight steady-state inaccuracy in real power effectiveness.

Moreover, Salp swarm optimization yields a superior outcome with less overshooting, a settling time of 0.03 ms, as well as a slight steady-state inaccuracy in reactive power efficiency. PI, GA and PSO, on the other hand, provide settling times of 0.12 ms and 0.08 ms, respectively. Consequently, the suggested Salp swarm optimization outperforms the other controllers. In other terms, the Salp swarm optimization produces a quicker and smoother output of real and reactive power than the other control approaches. Furthermore, the proposed controllers have the smallest peak overshoots and settling time among the different controllers.

5 Real-Time Investigation

A 2kVA grid-connected SPV is intended to study the reactive power capabilities of the system promptly. The suggested controllers are implemented in real-time using a Texas Devices 32-bit TMS310F28169 microcontroller. This study regulates real and reactive power individually to accomplish grid standards. In this research, the real power

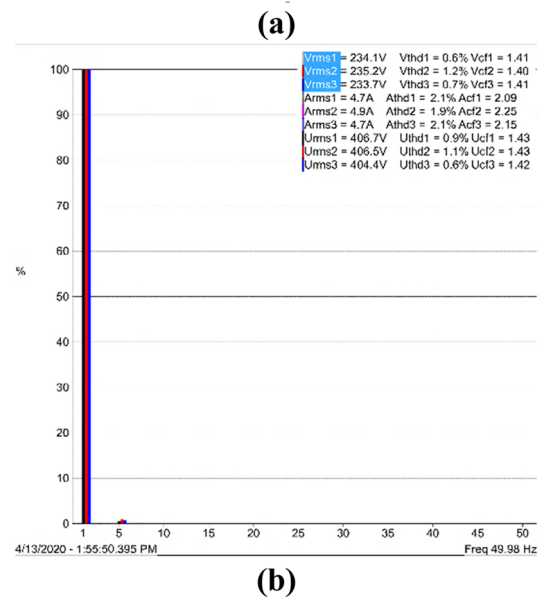
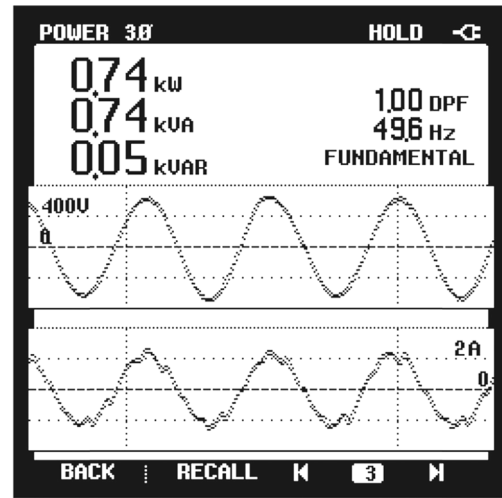
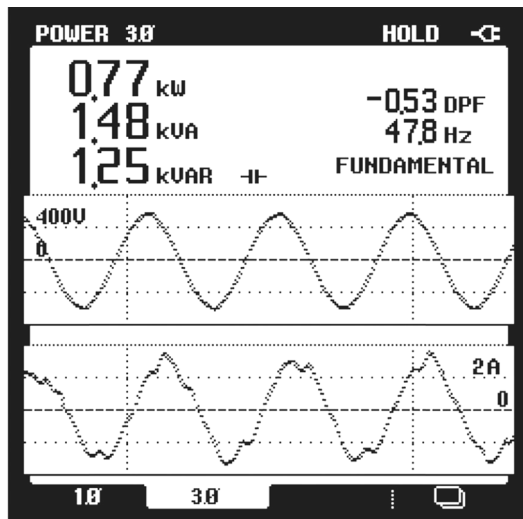


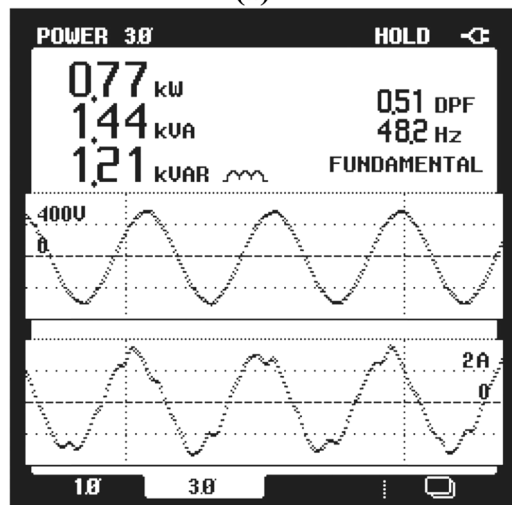
Fig. 19 Experimental results of the grid-tied inverter at UPF condition **a** power analysis, **b** current THD

reference is set to its highest level, and the reactive power is changed according to grid requirements. Figure 18 depicts the Solar PV, controller, and measuring devices. Reactive power evaluation requires real peak power to accomplish the UPF conditions. By fulfilling the UPF condition, the inverters deliver the real peak power of 0.74 kW with low reactive power of 0.05kVAR, as shown in Fig. 19. A reference value is set to a negative number to test the system’s reactive power absorption.

As a result, the system’s reactive power is 1.48 kVA, with overall apparent power of 1.25 kVAR, as shown in Fig. 20a. Ultimately, by setting the reactive power references to



(a)



(b)

Fig. 20 Experimental results of reactive power **a** absorption, **b** injection

positive, the system injects reactive power while maintaining the leading power factor. Consequently, the system injects 1.44kVA of reactive power with overall apparent power of 1.21 kVAR, as shown in Fig. 20b.

Furthermore, in the minimum irradiation state, performances are measured during 5.10 p.m., and the measured current Harmonic distortion of 5.9 percent is shown in Fig. 21. As a result, the investigation demonstrated that the voltage and the current Harmonic distortion levels are within allowable levels in the presence of reactive power injection and absorption.

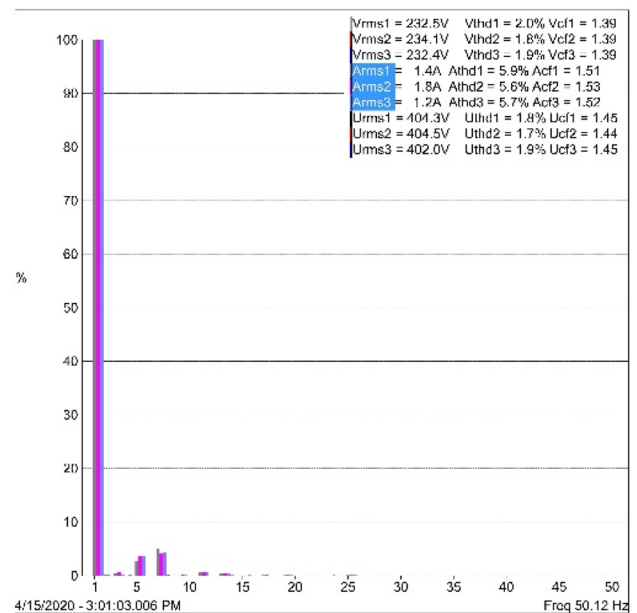


Fig. 21 Current THD plot at low power injection

6 Conclusion and Future Scope

The recommended research can improve power quality in production and distribution systems. Additionally, the suggested approach can regulate P–Q during the day. The grid voltage could be maintained by operating in VAR modes due to the lack of a solar PV inverter. Using Salp swarm optimization, the decoupled P–Q theory preserves the system’s reactive power capability. The power quality evaluation is performed in various circumstances to ensure the overall system’s performance. Current and voltage Harmonic distortion results in reactive power injection and absorption are lower than in typical feedforward architecture. The simulated results suggest that the Salp swarm optimization is more efficient and quicker than the other algorithms. In addition, the proposed research includes precise analysis to ensure performance. During the Absorption of Reactive Power (Q-Negative) with different types of controllers, for $P = 74.97$ kW, $Q = -75$ kW, the proposed technique generates a Voltage THD of 0.11 and Current THD of 0.29. During the Injection of Reactive Power (Q-Positive) with different types of controllers, for $P = 74.76$ kW and $Q = 75.01$ kW, the proposed technique generates a Voltage THD of 0.12 and Current THD of 0.66, respectively. During the Peak real power injection with different types of controllers, for $P = 75.02$ kW and $Q = 0.025$ kW, the proposed technique generates a Voltage THD of 0.12 and Current THD of 0.57, respectively. During the Night mode operation with different types of

controllers, for $P = -0.01$ kW, $Q = 75$ kW, the proposed technique generates a Voltage THD of 0.11 and Current THD of 0.53, respectively. The suggested approach improves power quality under lower power generation and low irradiation situations, yielding 3.64 percent in simulations and 5.6 percent in real-time.

Furthermore, the proposed grid-connected PV inverter could correct P–Q issues on the distribution system effectively and affordably. As a result, the suggested controller is regarded as an intelligent control system providing optimal P–Q regulation. This study may in future also be applied to additional P–Q issues using alternative artificial intelligence techniques with more analysis and comparison with trending methodologies.

Conflict of interest The authors declared that they have no conflicts of interest to this work.

References

- Singh R, Bansal RC, Singh AR, Naidoo R (2018) Multi-objective optimization of hybrid renewable energy system using reformed electric system cascade analysis for islanding and grid connected modes of operation. *IEEE Access* 6:47332–47354. <https://doi.org/10.1109/ACCESS.2018.2867276>
- Stonier AA, Murugesan S, Samikannu R et al (2020) Power quality improvement in solar fed cascaded multilevel inverter with output voltage regulation techniques. *IEEE Access* 8:178360–178371. <https://doi.org/10.1109/ACCESS.2020.3027784>
- Dolara A, Grimaccia F, Mussetta M et al (2018) An evolutionary-based MPPT algorithm for photovoltaic systems under dynamic partial shading. *Appl Sci*. <https://doi.org/10.3390/app8040558>
- Asef P, Perpina RB, Barzegaran MR, Laphorn A (2019) A 3-D pareto-based shading analysis on solar photovoltaic system design optimization. *IEEE Trans Sustain Energy* 10:843–852. <https://doi.org/10.1109/TSTE.2018.2849370>
- Alturki FA, Omotoso HO, Al-Shamma'AA et al (2020) Novel manta rays foraging optimization algorithm based optimal control for grid-connected PV energy system. *IEEE Access* 8:187276–187290. <https://doi.org/10.1109/ACCESS.2020.3030874>
- Chen J, Yue D, Dou C et al (2021) Distributed control of multi-functional grid-tied inverters for power quality improvement. *IEEE Trans Circuits Syst I Regul Pap* 68:918–928. <https://doi.org/10.1109/TCSI.2020.3040253>
- Koutroulis E, Yang Y, Blaabjerg F (2019) Co-design of the pvarray and DC/AC inverter for maximizing the energy production in grid-connected applications. *IEEE Trans Energy Convers* 34:509–519. <https://doi.org/10.1109/TEC.2018.2879219>
- Zidane TEK, Adzman MR, Tajuddin MFN et al (2021) Identifiability evaluation of crucial parameters for grid connected photovoltaic power plants design optimization. *IEEE Access* 9:108754–108771. <https://doi.org/10.1109/ACCESS.2021.3102159>
- Priyadarshi N, Padmanaban S, Bhaskar MS et al (2020) A hybrid photovoltaic-fuel cell-based single-stage grid integration with Lyapunov control scheme. *IEEE Syst J* 14:3334–3342. <https://doi.org/10.1109/JSYST.2019.2948899>
- Farah L, Hussain A, Kerrouche A et al (2020) A highly-efficient fuzzy-based controller with high reduction inputs and membership functions for a grid-connected photovoltaic system. *IEEE Access* 8:163225–163237. <https://doi.org/10.1109/ACCESS.2020.3016981>
- Islam MR, Lu H, Islam MR et al (2020) An IoT-based decision support tool for improving the performance of smart grids connected with distributed energy sources and electric vehicles. *IEEE Trans Ind Appl* 56:4552–4562. <https://doi.org/10.1109/TIA.2020.2989522>
- Shafi A, Sharadga H, Hajimirza S (2020) Design of optimal power point tracking controller using forecasted photovoltaic power and demand. *IEEE Trans Sustain Energy* 11:1820–1828. <https://doi.org/10.1109/TSTE.2019.2941862>
- Benali A, Khiat M, Allaoui T, Denai M (2018) Power quality improvement and low voltage ride through capability in hybrid wind-PV farms grid-connected using dynamic voltage restorer. *IEEE Access* 6:68634–68648. <https://doi.org/10.1109/ACCESS.2018.2878493>
- Beniwal RK, Saini MK, Nayyar A et al (2021) A critical analysis of methodologies for detection and classification of power quality events in smart grid. *IEEE Access* 9:83507–83534. <https://doi.org/10.1109/ACCESS.2021.3087016>
- Moghassemi A, Padmanaban S, Ramachandaramurthy VK et al (2021) A novel solar photovoltaic fed TransZSI-DVR for power quality improvement of grid-connected PV systems. *IEEE Access* 9:7263–7279. <https://doi.org/10.1109/ACCESS.2020.3048022>
- Jayachitra A, Vinodha R (2014) Genetic algorithm based PID controller tuning approach for continuous stirred tank reactor. *Adv Artif Intell* 2014:1–8. <https://doi.org/10.1155/2014/791230>
- Roslan MF, Al-Shetwi AQ, Hannan MA et al (2020) Particle swarm optimization algorithm-based PI inverter controller for a grid-connected PV system. *PLoS ONE* 15:e0243581
- Ceylan O (2021) Multi-verse optimization algorithm- and salp swarm optimization algorithm-based optimization of multilevel inverters. *Neural Comput Appl* 33:1935–1950. <https://doi.org/10.1007/s00521-020-05062-8>

Publisher's Note Springer Nature remains neutral with regard to jurisdictional claims in published maps and institutional affiliations.

Springer Nature or its licensor (e.g. a society or other partner) holds exclusive rights to this article under a publishing agreement with the author(s) or other rightsholder(s); author self-archiving of the accepted manuscript version of this article is solely governed by the terms of such publishing agreement and applicable law.



N. Vanaja received the B.E. degree in Electrical and Electronics Engineering in 2017 and received Master of Engineering in Power Electronics and Drives in 2009 from Anna University, Chennai, Tamil Nadu, India. She is currently working as an Assistant Professor in Electrical Engineering Department at Mepco Schlenk Engineering, Sivakasi, India and pursuing her research in the domain of Optimization of Renewable Energy Sources Integration to Smart Grid under Anna University,

Chennai, India. Her research interests are on Power Electronics, Controllers, Fuzzy and neural networks and Smart Grid.



N. Senthil Kumar obtained his B.E. degree in Electronics and Communication Engineering from Madurai Kamaraj University, Madurai, in 1988, M.E. degree in Electronics Engineering from Anna University, Chennai, in 1991 and Ph.D. in Electronics and Computer Science engineering from Manonmaniam Sundaranar University, Tirunelveli in 2008. Currently, he is working as a Senior Professor and Head in department of Electrical and Electronics Engineering at Mepco Schlenk Engi-

neering College (Autonomous), Sivakasi, India. He has published a paper in National Journal and 55 papers in International Journals. His

interests include Electronics Engineering, Power Converters, Microprocessors, Microcontrollers, Embedded Systems, Fuzzy and neural networks, Control systems. He is a member of FIE, IEEE, IETE, ISTE and SSI.